SCIENTIFIC REPORTS
nature research

OPEN

B4GALNT1 induces angiogenesis, anchorage independence growth and motility, and promotes tumorigenesis in melanoma by induction of ganglioside GM2/GD2

Hideki Yoshida[1], Lisa Koodie[1], Kari Jacobsen[1], Ken Hanzawa[2], Yasuhide Miyamoto[2] & Masato Yamamoto[1,3,4*]

β-1,4-N-Acetyl-Galactosaminyltransferase 1 (B4GALNT1) **encodes the key enzyme B4GALNT1 to generate gangliosides GM2/GD2. GM2/GD2 gangliosides are surface glycolipids mainly found on brain neurons as well as peripheral nerves and skin melanocytes and are reported to exacerbate the malignant potential of melanomas. In order to elucidate the mechanism, we performed functional analyses of B4GALNT1-overexpressing cells. We analyzed ganglioside pattern on four melanoma and two neuroblastoma cell lines by high performance liquid chromatography (HPLC). We overexpressed B4GALNT1 in GM2/GD2-negative human melanoma cell line (SH4) and confirmed production of GM2/GD2 by HPLC. They showed higher anchorage independence growth (AIG) in colony formation assay, and exhibited augmented motility. *In vitro*, cell proliferation was not affected by GM2/GD2 expression. *In vivo*, GM2/GD2-positive SH4 clones showed significantly higher tumorigenesis in NOD/Scid/IL2Rγ-null mice, and immunostaining of mouse CD31 revealed that GM2/GD2 induced remarkable angiogenesis. No differences were seen in melanoma stem cell and Epithelial-Mesenchymal Transition markers between GM2/GD2-positive and -negative SH4 cells. We therefore concluded that B4GALNT1, and consequently GM2/GD2, enhanced tumorigenesis via induction of angiogenesis, AIG, and cell motility. RNA-Seq suggested periostin as a potential key factor for angiogenesis and AIG. These findings may lead to development of novel therapy for refractory melanoma.**

Malignant melanoma is the most common and lethal skin cancer[1,2]. It is a cancer with one of the biggest rise in incidence[3,4], and the overall 5-year survival rate is less than 10% for patients with stage IV disease[5,6]. There have been major advances in the treatment of advanced melanoma including Ipilimumab, an antibody to cytotoxic T-lymphocyte-associated-antigen-4 (CTLA-4), and BRAF inhibitor[7–9]. However, the anti-CTLA-4 antibody shows benefit in less than 50% of patients[10]. While BRAF inhibitors increased survival compared to other chemotherapies, its indication is limited to about half of patients with BRAF V600 mutations, and almost all patients develop resistance to these inhibitors[11]. While the combination of Nivolumab (monoclonal antibody against programmed death 1, PD-1) and Ipilumumab has demonstrated an impressive 2-year overall survival rate of 63.8% in stage III-IV patients[12], further improvement of therapy is still needed for the treatment of advanced melanoma patients.

β-1,4-N-Acetyl-Galactosaminyltransferase 1 (B4GALNT1) encodes B4GALNT1 (GM2/GD2 synthase), and it works as the key enzyme which transfers a N-acetylgalactosamine (GalNAc) to GM3/GD3, yielding gangliosides GM2/GD2 as part of their stepwise synthesis (Fig. 1A). Gangliosides, including GM2 or GD2, belong to the family of glycosphingolipids (GSL) and contain one or more sialic acids, N-acetyl derivatives of neuraminic acid, in their hydrophilic oligosaccharide chain.[13] Gangliosides are sialic acid-containing glycosphingolipids that are most

[1]Department of Surgery, University of Minnesota, Minneapolis, Minnesota, USA. [2]Department of Molecular Biology, Osaka International Cancer Institute, Osaka, Japan. [3]Masonic Cancer Center, University of Minnesota, Minneapolis, Minnesota, USA. [4]Stem Cell Institute, University of Minnesota, Minneapolis, Minnesota, USA. *email: yamam016@umn.edu

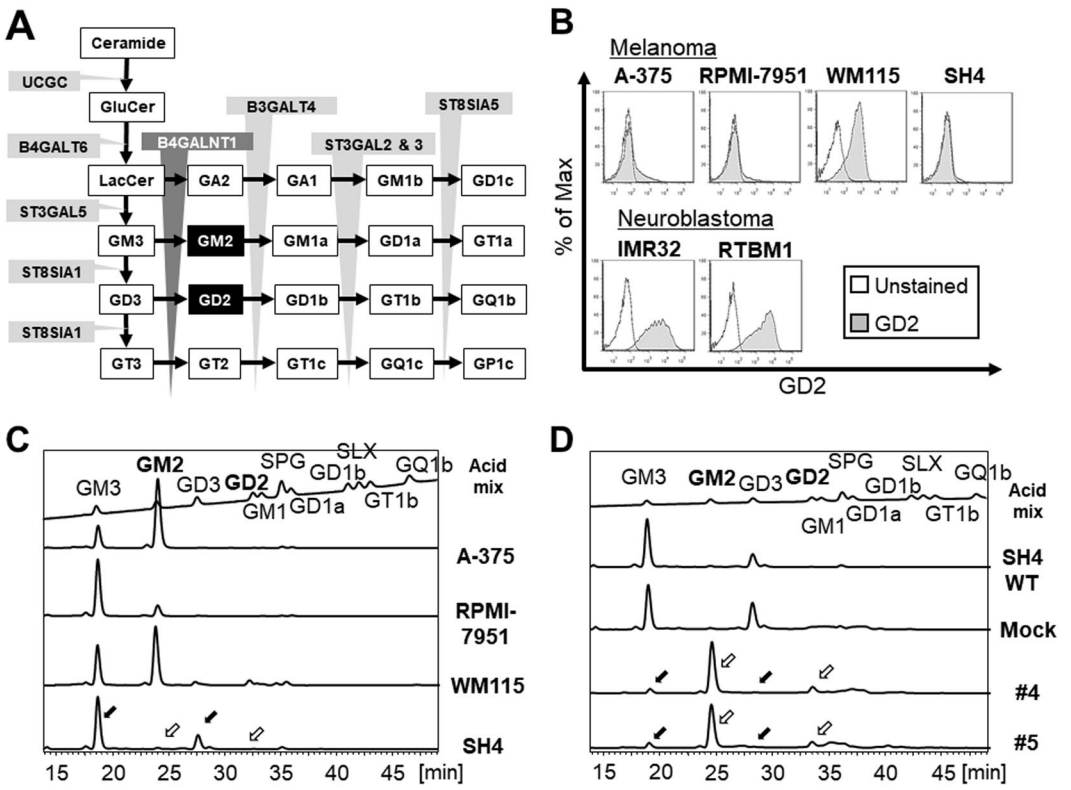

Figure 1. Schemes of ganglioside synthesis and analyses of gangliosides in the cells. (**A**) Glycosylation sequences for biosynthesis of GM2/GD2. B4GALNT1 (*β-1,4-N-Acetyl-Galactosaminyltransferase 1*) is the critical enzyme for the GM2/GD2 synthesis. (**B**) Flow cytometry Analysis of GD2 on the cultured cells; four human melanoma cell lines (A375, RPMI-7951, WM-115 and SH4), and two human neuroblastoma cell lines (IMR32 and RTBM1). (**C**) Detail analysis of acidic gangliosides on the four melanoma cell lines. The surface expression of gangliosides was analyzed by HPLC. Y-axis indicated intensity of fluorescence. (**D**) HPLC-based analysis of acidic gangliosides on SH4 cell line before and after B4GALNT1 overexpression. Mock is SH4 with pcDNA3.1(+) expression vector alone. #4 and #5 single cells are isolated SH4 clones with B4GALNT1 overexpression. Black arrows; GM3/GD3, white arrows; GM2/GD2.

abundant in the nervous system, especially brain neurons[14]. They also exist in peripheral nerves and skin melanocytes[15,16]. These molecules are reported to have important biological functions, such as intercellular communication, cell cycling, cell growth, adhesion, differentiation, and cell motility[17–19]. Gangliosides are not only detected at high levels in tumors of neuroectodermal cell origin but also related to the biological and clinical behavior of many kinds of tumors[20]. Recently, some analysis revealed that patients with higher expression of B4GALNT1 and GM2/GD2 correlated with poorer prognosis in renal cell carcinoma (TCGA data set; Human Protein Atlas), neuroblastoma[21], and melanoma[22]. Thus, B4GALNT1 gene is considered to be key tumor-associated antigens[23–27], indicating that their expression is a meaningful marker for metastatic condition and are potential therapeutic targets for melanoma.

Our findings indicate the involvement of B4GALNT1 and GM2/GD2 in tumor establishment and progression as well as a potential direction of therapeutic approach *via* controlling B4GALNT1, and consequently GM2/GD2 expression in cancers such as melanoma.

Results

GM2/GD2 expression status in melanoma and neuroblastoma cell lines. To assess the GM2/GD2 expression level, four melanoma (A-375, RPMI-7951, WM115 and SH4) and two neuroblastoma cell lines (IMR32 and RTBM1) were measured by flow cytometry. One melanoma (WM115) and both of two neuroblastoma cell lines expressed high level of GM2/GD2 (Fig. 1B).

Because gangliosides including GM2/GD2 require stepwise synthesis reactions (Fig. 1A), a model for induced expression of GM2/GD2 on cell surface via overexpression of B4GALNT1 needs the following conditions; 1) both GM3 and GD3 are positive, and 2) both GM2 and GD2 are negative. To evaluate these conditions accurately in the six cell lines, HPLC-based high-specificity analysis of gangliosides was performed (Fig. 1C). Being that SH4 melanoma cell line showed high expression of both GD3 and GM3 (black arrows) and no expression of GD2 and GM2 (white arrows), SH4 fulfilled the aforementioned conditions and was used in the following study. Other results of neuroblastoma cells were shown in Fig. S1.

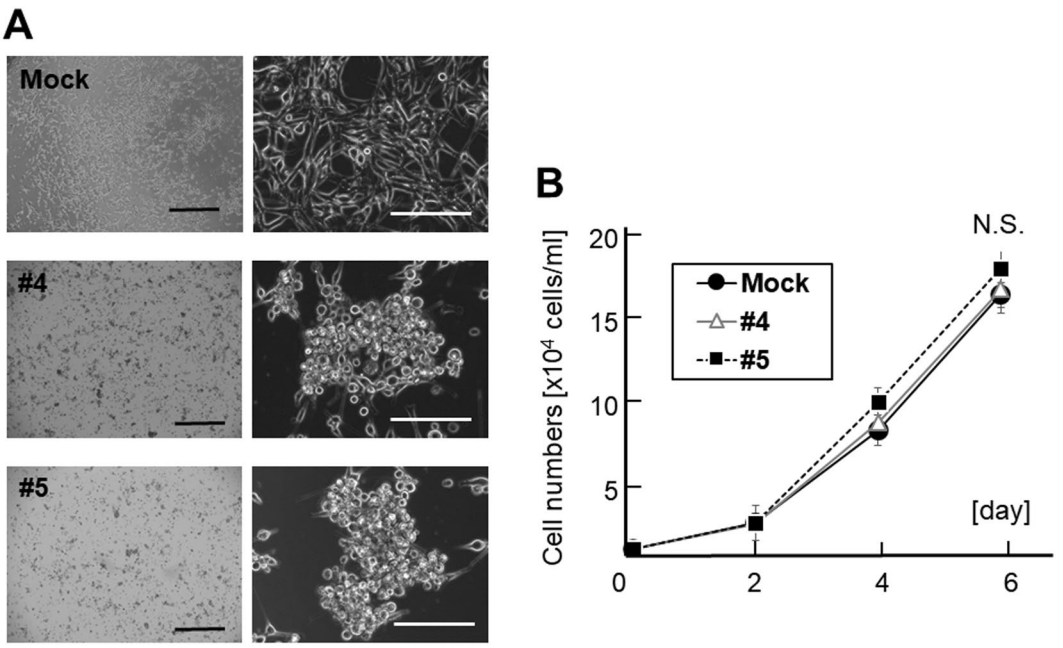

Figure 2. Effect of B4GALNT1 overexpression on cell morphology and growth. (**A**) Morphological changes in SH4 after B4GALNT1 overexpression. Scale bar, 1,000 μm (left) and, 200 μm (right). (**B**) Cell growth of SH4 with or without GM2/GD2-expression 6 days later. Results represent the means ∓ s.d. from three independent experiments.

Generation of GM2/GD2-positive SH4 melanoma clones. The SH4 cells were transfected with expression vectors with or without *B4GALNT1* gene cassette, to establish GM2/GD2-positive and -negative SH4 clones. Two GM2/GD2-high clones were selected by single cell isolation (#4 and #5, Fig. S2A). These two clones showed significant expression of GD2, whereas Mock (pcDNA3.1(+) alone) and two clones showed no GD2 expression. The expressions of *B4GALNT1* in mRNA level were in correspondence with those by flow cytometry (Fig. S2B). Additionally, HPLC revealed that the clones #4 and #5 expressed GM2/GD2 at high level (Fig. 1D). The reason that GD2 level in the transfected clones is very low compared to the GD3 level in the parental cells was interpreted that B4GALNT1 and ST8Sia1 competes GM3 as a substrate. It is known that GD2 is not synthesized from GM2[28].

Induction of morphological change, anchorage independence growth, and cell motility. The SH4 clones overexpressing GM2/GD2, #4 and #5, exhibited a distinct morphological appearance compared to SH4 Wild type (WT) or the mock transduced cells. The cells were round and formed aggregation. More than half of them were detached from the bottom of flask, but still capable of survival and proliferation after detachment (Fig. 2A). No significant difference was seen between the proliferation of GM2/GD2-positive SH4 clones and control (Fig. 2B). A soft agar colony formation assay demonstrated that GM2/GD2-positive SH4 clones formed larger and greater number of colonies than GM2/GD2-negative cells (#4; 86.6 ± 13.9, #5; 82.5 ± 6.5, Mock; 32.7 ± 6.6, #4 vs Mock; $p < 0.0001$, #5 vs Mock; $p < 0.0001$, Fig. 3A). There was no significant difference between the two GM2/GD2-positive SH4 clones (#4 vs #5; $P = 0.15$). In addition, faster wound closure was observed in the GM2/GD2-positive SH4 clones than the control cells (#4: 49.7 ± 16.4 vs #5: 56.5 ± 25.3 vs Mock: 85.9 ± 14.8, #4 vs Mock: $p < 0.0001$, #5 vs Mock: $p < 0.0001$, #4 vs #5: $p = 0.98$, Fig. 3B,C), indicating enhanced motility.

Enhancement of tumor incidence and growth speed *in vivo*. To assess the *in vivo* effect of GM2/GD2 induced by B4GALNT1 overexpression, the two GM2/GD2-positive SH4 clones and Mock were inoculated in NOD/Scid/IL2Rγ-null (NSG) mice to assess tumor initiation and growth. After transplanting 2×10^6 GM2/GD2-positive and -negative SH4 cells, all mice receiving #4 and #5 cells developed tumors, whereas only three out of six mice injected with Mock cells developed tumors ($P = 0.038$, Fig. 4A, Table 1). In the NSG mice transplanted with lower number (2×10^5) of GM2/GD2-positive or -negative SH4 cells, seven out of eight mice injected with #4 and #5 cells developed tumors, whereas two out of six mice injected with Mock cells developed tumors ($P = 0.038$, Fig. 4B, Table 1). Moreover, in the NSG mice transplanted with 2×10^6 GM2/GD2-positive or -negative SH4 cells, tumors derived from GM2/GD2-positive cells grew to be approximately three times larger than the GM2/GD2-negative Mock at day 54 (9.4 ± 1.9 vs 3.2 ± 3.5 mm, $P = 0.003$, Fig. 4A). In the NSG mice transplanted with 2×10^5 GM2/GD2-positive or -negative SH4 cells, tumors derived from GM2/GD2-positive cells grew to be over three times as large as those from GM2/GD2- negative Mock in 54 days (4.0 ± 1.8 vs 1.1 ± 1.8 mm, $P = 0.026$, Fig. 4B). Every tumor was solid, firm, and partially fibrotic.

No evident difference in major cancer stem cell markers. To evaluate the possibility that B4GALNT1 overexpression might enhance tumor incidence via induction of stemness, several melanoma stem cell markers were analyzed in GM2/GD2- positive and -negative cells by flow cytometry. Previous reports indicated that

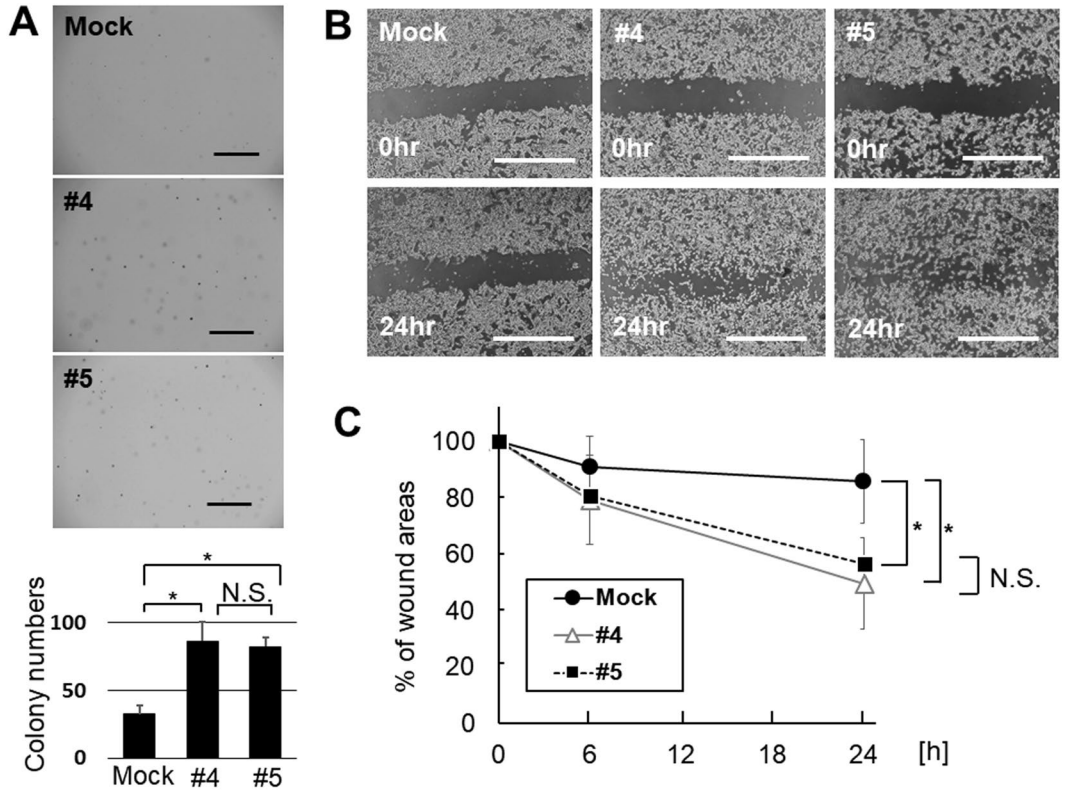

Figure 3. Effect of B4GALNT1 overexpression to cell behavior. (**A**) Photographs of colonies of SH4 cells with and without B4GALNT1 overexpression 14 days later. Scale bar, 1,000 μm. Results represent the means ∓ s.d. of three independent experiments. (**B**) Light microscopic images of SH4 cells that were scratched and compared the wound width 6 and 24 h later. Scale bar, 1,000 μm. (**C**) Average wound widths, expressed as a percent of the original width, obtained from 30 measurements in each photo. Results represent the means ∓ s.d. of three independent experiments. *$P < 0.01$ compared with Mock. N.S.; Not Significant.

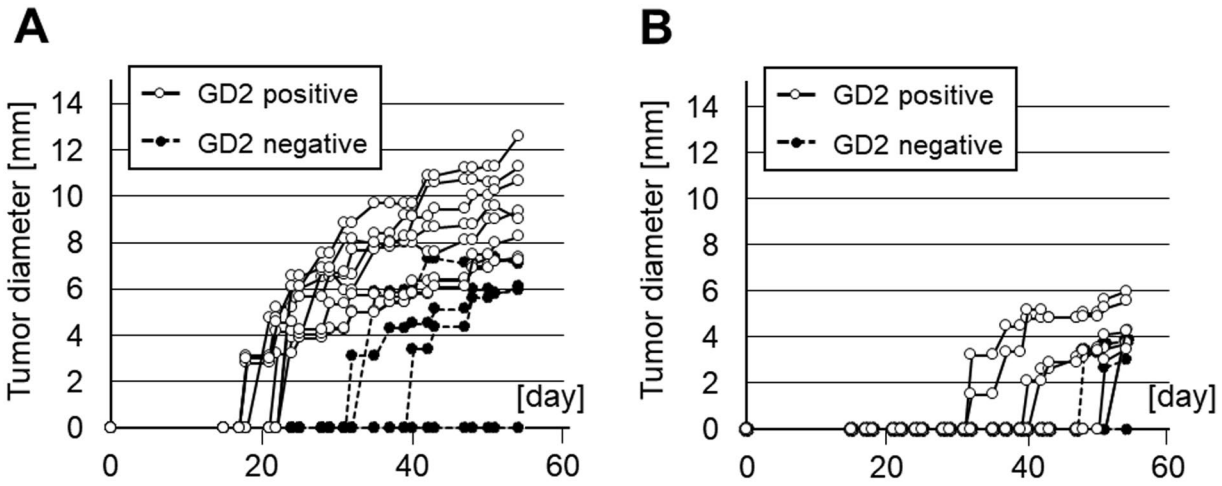

Figure 4. Effects of B4GALNT1-overexpressing on the proliferation of SH4 cells in xenograft models. (**A**) 2×10^6, (**B**) 2×10^5 SH4 cell were inoculated into lower flank of NSG mice subcutaneously.

		GM2/GD2		
		positive	negative	p-value
cell	2×10^6	8/8	3/6	$P < 0.05$
number	2×10^5	7/8	2/6	$P < 0.05$

Table 1. Tumor incidence *in vivo*.

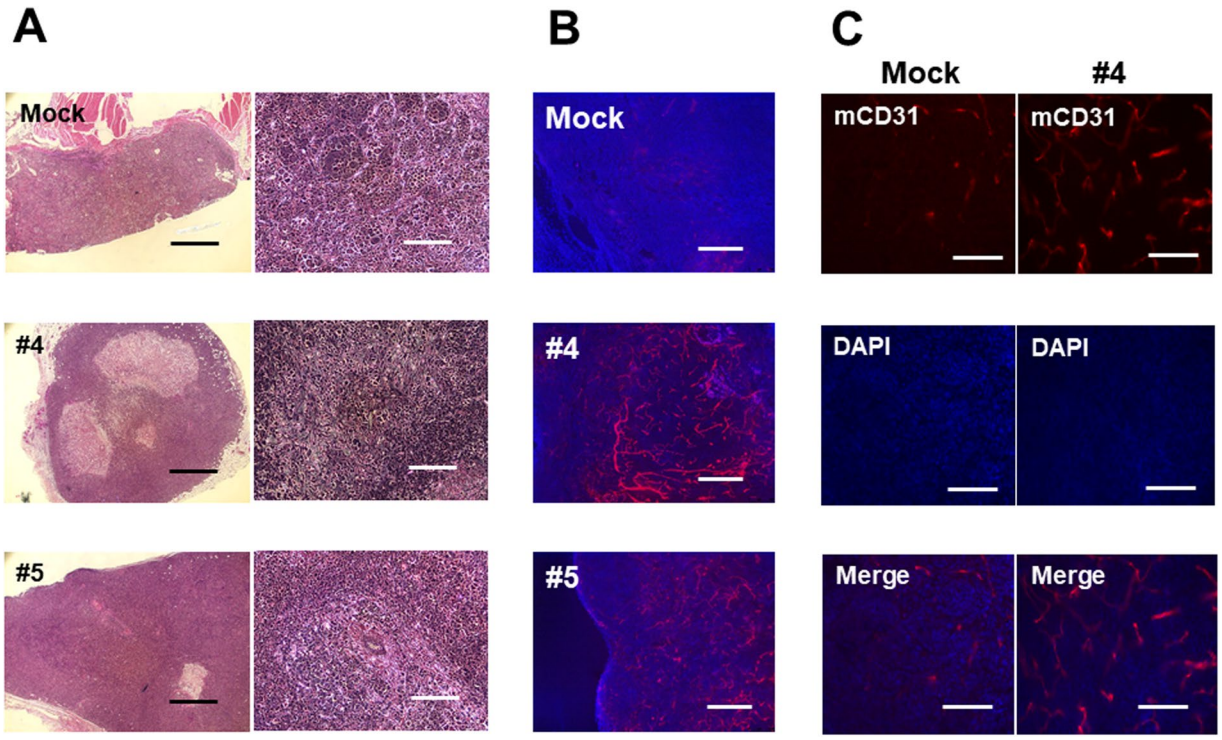

Figure 5. Histological analyses of the tumors. (**A**) Images of tissue sections of SH4 (H&E). (**B**,**C**) Immunostaining with murine CD31. Scale bar, 1,000 μm (**A**; left), 200 μm (**A**; right), 400 μm (**B**), and 100 μm (**C**), respectively.

CD133[29–31], CD166[29], CD271[32], Nestin[30],and ABCB5[33] are potential melanoma stem cell markers. Aldehyde dehydrogenase (ALDH) activity has also been reported as a potential marker of melanoma stem cell[34]. However, B4GALNT1 overexpression did not induce any meaningful change in any of these markers (Fig. S3A–F), there was no significant difference in CD133, CD166, and ABCB5 between GM2/GD2-positive and -negative cells. There was a small decrease in the expression of CD271 and Nestin in the #5 GM2/GD2-positive cell line, but this alone is unlikely to be the cause of enhanced tumor growth. That indicated that B4GALNT1 was unlikely to affect the stemness in the SH4 melanoma cell line.

Promotion of angiogenesis *in vivo*. We hypothesized that B4GALNT1 may enhance tumor induction and growth by increasing tumor vascularization. Tumors of similar size from each group were stained by hematoxylin and eosin (H&E) and immunofluorescence for murine-CD31. In H&E staining, the tumors induced by GM2/GD2-positive or -negative SH4 cells did not differ in any characteristics examined: cell shape, number of giant cells, nuclear-to-cytoplasm volume ratio reversal, and hyperchromatism (Fig. 5A). The major blood vessel in the GM2/GD2-positive tumors were more prominent than the one supplying the Mock tumor. Although some tumors showed evidence of local invasion, none of the tumor-bearing mice developed metastasis.

Immunofluorescence staining in tumors derived from GM2/GD2-positive clones by anti-mouse CD31 Ab exhibited many well-structured vessels, while GM2/GD2-negative Mock tumors had much less (Fig. 5B,C). Immunofluorescence performed using selective anti-human-CD31 antibody (non-reactive to mouse CD31) as a negative control did not show any staining of blood vessels (data not shown).

RNA-Seq revealed potential key molecule downstream of B4GALNT1. To identify the difference of the transcriptional profile between GM2/GD2-positive and -negative cells, we compared them by RNA-Seq and analyzed using edgeR. There were a total of 26,484 genes detected in the individual libraries (Table S1), and 472 genes showed over +/− two-fold change between the two groups (Table S2). The heat map was shown in Fig. S4A. Among the 472 genes, 117 genes were up-regulated and 351 genes were down-regulated by B4GALNT1 overexpression. There was no significant difference between the two Mock clones (Fig. S4B), as well as between two GM2/GD2-positive samples (#4 and #5 clones; Fig. S4C). Genes exhibiting the Top 10 largest fold changes are listed in Table 2. The top up-regulated gene, *PTPRD*, is a member of the protein tyrosine phosphatase (PTP) family, and is known to be a signaling molecule that regulates a variety of cellular processes including cell growth, differentiation as a tumor suppressor[35], which was often down-regulated in a variety of tumors. The second highest was *B4GALNT1*, suggesting that our overexpression of the gene in SH4 had succeeded. The third highest, *POSTN* (periostin), functions as a ligand for alpha-V/beta-3 and alpha-V/beta-5 integrins to support adhesion and migration[36–38]. In addition, it is known to increase angiogenesis. Furthermore, *CPVL* (Carboxypeptidase Vitellogenic Like), the top down-regulated gene was related to maturation of monocytes into macrophages[39]. Carboxypeptidases are a large class of proteases that act to cleave a single amino acid from the carboxy termini

Symbol	Gene name	Expr Fold change	p-value
Up-regulation			
PTPRD	Protein tyrosine phosphatase receptor type D	735.0563	0.005722
B4GALNT1	Beta-1,4-N-acetyl- galactosaminyltransferase 1	359.3801	1.4E-150
POSTN	Periostin	286.3453	4.95E-26
SERPINB2	Serpin family B member 2	240.9988	7.94E-06
HLA-DRB1	human leukocyte antigen, class II, DR beta 1	228.4819	1.07E-05
IL13RA2	Interleukin 13 receptor alpha 2	191.2431	0.000616
CSMD1	CUB and sushi multiple domains 1	188.313	7.75E-05
MYBPC1	Myosin binding protein C type 1	182.0119	0.000805
ADGRL2	Adhesion G protein- coupled receptor L2	158.3556	4.73E-92
TNFRSF14	TNF receptor superfamily member 14	142.9792	0.011144
Down-regulation			
CPVL	Carboxypeptidase vitellogenic like	−1370.3	3.27E-37
MAGEA12	Melanoma-associated antigen 12	−1143.23	9.84E-16
CSAG1	Chondrosarcoma associated gene 1	−676.619	8.41E-12
GIPC3	PDZ domain containing family Member 3	−535.495	1.85E-20
CPM	Carboxypeptidase M	−484.607	3.42E-15
ZXDA	Zinc finger, X-linked, duplicated A	−457.61	9.68E-09
FAM83H	Family with sequence similarity 83	−412.334	1.45E-08
PRAME	Preferentially expressed antigen in melanoma	−411.078	0.000851
GABRQ	Gamma-aminobutyric acid type A receptor theta subunit	−402.747	1.57E-21
LDB2	LIM domain binding 2	−371.463	0.000011

Table 2. Top 10 of the greatest genes expression changes in SH4 with vs without GM2/GD2.

of proteins or peptides. The exact function of this protein, however, has not been determined. The second and third downregulated genes were melanoma-associated antigen 12 (*MAGEA12*[40]) and chondrosarcoma associated Gene 1 (*CSAG1*[41]) which are oncogenes, supposed to be overexpressed in tumors, but in this case they were down-regulated upon *B4GALNT1* overexpression.

To further elucidate the role of the 472 genes, we categorized them by function related to cancer malignancy using Ingenuity Pathway Analysis (IPA). This included several genes that functioned as melanoma incidence, proliferation, mobility and colony formation. Some genes were up- or down-regulated as the past reports and others were not (Table 3; "*" means that the fold changes went the opposite direction compared with previous findings). Some of them changed in the opposite direction compared to past reports in melanoma carcinogenesis. These genes may not function as downstream of B4GALNT1, and may have shown a change opposite of other literature due to negative feedback. Pathway analysis was attempted, but no known pathway was found that could fully explain our expression profile suggesting that the revelation of the pathway downstream of glycolipids is not complete.

Discussion

In this study, we analyzed a variety of changes in the SH4 melanoma cell line upon overexpression of GM2/GD2 by transfection of *B4GALNT1 gene*. One of remarkable findings *in vitro* is that GM2/GD2-positive SH4 cells showed significant difference of AIG compared to Mock (Fig. 3A), interestingly, Mahata *et al*. also revealed that GM2/GD2 is associated with AIG by knocking out GM2/GD2 synthase[42]. AIG is often reported as a critical factor for tumorigenesis or exacerbation of malignancy[42–44]. Although we initially expected contribution of Epithelial-Mesenchymal Transition (EMT), neither *CDH1* (E-cadhelin) nor *VIM* (vimentin), the major EMT markers, showed change at the mRNA level (data not shown). On the other hand, our RNA-Seq result showed that the expression of *POSTN* in B4GALNT1-overexpressing cells increased by almost 300 times than Mock cells. Periostin is generally known as a cancer suppresser[45] and it also help to migration in neuronal cell development[46]. While periostin is involved in numerous biological processes, it sometimes contributes to tumorigenesis by promoting cancer cell survival, invasion, and metastasis actively[36–38]. It is also known that high expression of periostin protein and/or mRNA is detected in variety of solid tumors[38,47]. Kudo *et al*. showed that periostin overexpression promoted invasion in head and neck squamous cell carcinoma cells[48] and to explore the genes that are coordinately expressed with periostin, they performed microarray analysis. Among the genes changed in their study, *SULF1* was upregulated clearly in our result as well (9.30-fold; Table S2). On top of that, Kotbuki *et al*. directly revealed that periostin increased cell proliferation and invasion in melanoma cell *in vitro* and *in vivo* using overexpression system[49], and Fukuda *et al*. showed that periostin was a key factor in promoting melanoma cell metastasis using shRNA[50]. We therefore speculated that the findings support our conclusion that periostin and its downstream gene overexpression promoted migration induced by GM2/GD2. Furthermore, Bao *et al*. demonstrated that periostin activated the downstream Akt/PKB pathway *via* $\alpha v\beta 3$ integrin, by in which they observed phosphorylation of Akt1/PKBα on Ser473 to promote cellular survival in colon cancer[51]. Their phosphorylation level, not the total amount, would therefore be contributing to the downstream effect of GM2/GD2. This may explain why our RNA-Seq result did not show a remarkable fold change in Akt/PKB pathway (Table S1).

Symbol	Expr Fold change	findings	Symbol	Expr Fold change	findings
Up-regulatation			**Down-regulated**		
Invasion of tumor					
POSTN	286.345	Increases	*EDN3*	−248.929	Decreases
NRP1	117.774	Increases	*VCAN**	−243.495	Increases
*IGFBP5**	26.687	Decreases	*IL24*	−15.763	Decreases
MMP1	20.329	Increases	*SERPINE1**	−9.371	Increases
*TGFBR2**	6.627	Decreases	*SFRP1*	−6.729	Decreases
ITGA1	4.868	Increases	*MMP2**	−6.046	Increases
TBX2	2.561	Increases	*GPC1**	−4.435	Increases
*HMGB3**	2.021	Decreases	*CEACAM1**	−4.131	Increases
SPHK1	2.012	Increases	*EGF**	−3.683	Increases
*CTGF**	−2.077	Decreases	*CSF1**	−2.879	Increases
Migration of melanoma cell					
*NRP1**	117.774	Decreases	*VCAN*	−243.495	Affects
SDC2	11.904	Increases	*L1CAM**	−20.041	Increases
TNC	2.217	Increases	*SERPINA5**	−10.969	Increases
SPHK1	2.012	Increases	*SERPINE1**	−9.371	Increases
			*MMP2**	−6.046	Increases
			*EGF**	−3.683	Increases
			*FN1**	−2.15	Increases
Cell proliferation of tumor cell lines					
POSTN	286.345	Increases	*PRAME**	−411.078	Increases
*SERPINB2**	240.999	Decreases	*VCAN**	−243.495	Increases
IL13RA2	191.243	Affects	*EMILIN2*	−124.892	Decreases
NRP1	117.774	Affects	*TRPM2**	−94.449	Increases
HTN1	60.939	Increases	*SYNM**	−26.275	Increases
*MAF**	50.99	Decreases	*PDGFB**	−22.149	Increases
POU4F1	50.781	Increases	*L1CAM**	−20.041	Increases
VIP	39.551	Increases	*CARD10**	−16.191	Increases
CDK14	30.195	Increases	*IL24*	−15.763	Decreases
IGFBP5	26.687	Increases	*S100A4**	−15.312	Increases
Colony formation					
POSTN	286.345	Affects	*VCAN**	−243.495	Increases
*HTN3**	98.45	Decreases	*NUPR1*	−31.659	Decreases
VIP	39.551	Increases	*PDGFB**	−22.149	Increases
TP63	8.144	Increases	*IL24*	−15.763	Decreases
CDCA7L	4.871	Increases	*S100A4**	−15.312	Increases
ITGA1	4.868	Increases	*SERPINE1*	−9.371	Decreases
ALDH1A1	4.81	Affects	*TBX3**	−7.463	Increases
HAS2	4.155	Increases	*DUSP5**	−6.896	Increases
TNC	2.217	Affects	*SFRP1**	−6.729	Increases
*LIMA1**	2.133	Decreases	*PTGES**	−6.519	Increases

Table 3. Gene expression characterestics. *means that the fold changes went the opposite direction compared with previous findings.

In our observation, B4GALNT1 overexpression did not affect cell proliferation *in vitro*, while multiple genes related to tumor cell proliferation-promoting, such as *POSTN, IL13RA2, NRP1* were up-regulated, and *EMILIN2*, which is a proliferation-suppressing gene, was down-regulated notably in mRNA level (Fig. 2B, Table 3). The relationship between ganglioside and cell proliferation is still controversial; some research suggest promotion of proliferation by gangliosides[52–54], while others show inhibition[55]. These discrepancies may be explained by the difference in the ratio of GD2 + 3 vs GM2 + 3, as well as GD2 vs GD3, which may contribute to differences in cell proliferation. The report by Shibuya *et al.* which induced GM2/GD2 like ours showed enhanced cell migration[55], similar to what we observed, supporting that B4GALNT1 and consequently GM2/GD2 intensified migration of SH4 cell (Fig. 3B). Periostin is known to promote motility of several different kinds of cells[56–58]. While our IPA analysis did not include the category of melanoma cell migration, RNA-Seq indicated that *SDC2* and *VCAN* might have led to the motility (Table 3).

Another finding was that GM2/GD2 strongly induced angiogenesis. The effect of B4GALNT1 for tumor incidence *in vivo* was assessed by injecting GM2/GD2-positive SH4 cells into NSG mice. As shown in Fig. 4A,B, the

tumors injected GM2/GD2-positive cells showed a higher tumor establishment rate. This result corresponds with the fact that *B4GALNT1* is a clinical marker for advanced melanoma[59]. Liu Y *et al*. revealed that gangliosides accelerate tumor angiogenesis in murine cells and demonstrated that GM2/GD2-negative cells formed much smaller tumors, using GM3 synthase and GM2 synthase double knockout low ganglioside tumor model[60]. We assessed murine-CD31 expression in the tumors derived from GM2/GD2-positive cell by immunofluorescence staining and observed that B4GALNT1-overexpressing clones induced many CD31 positive endothelial cells and well-developed vessels. In addition, the surface of the GM2/GD2-positive tumors were better vascularized than that of Mock by observation of the recovered tumor with eyes. Tumor progression requires endothelial cells to be activated for the formation of a vascular system. Lang Z *et al*. found that the enrichment of human umbilical vein endothelial cell (HUVEC) membranes with ganglioside results in amplified VEGF-induced signaling that is important for angiogenesis, and concluded that ganglioside enhances VEGF-induced endothelial cell proliferation[61]. Liu Y *et al*. reported that reduction of gangliosides depleted vascularization, while addition of wild type gangliosides restored angiogenesis of ganglioside-poor tumor[60]. To clarify how gangliosides induce blood vessels, we assessed the relations of GM2/GD2 and VEGF. Some other reports indicate that ganglioside enhances VEGF and induces endothelial cell proliferation[61,62]. In addition, Liu Y *et al*. also reported that periostin induces angiogenesis via Erk/VEGF pathway[63]. However, in our result of RNA-Seq and real-time RT-PCR, the expression of VEGF did not show significant correlation with GM2/GD2 level (Table S1, Fig. S5). There is a possibility that interaction between periostin and integrins directly promoted angiogenesis[64] or GM2/GD2 lowered the threshold for cytokine stimulation[60,65].

While GM2 and GD2 were reported to be increased greatly in cancer stem cells in breast cancer[66,67], our data ruled out the possibility that GM2/GD2 enhanced tumor incidence via induction of cell stemness. We assessed some melanoma stem cell markers, such as CD133, CD166, CD271, Nestin, ABCB5, and ALDH activity by flow cytometry, and there was no evidence indicative of GM2/GD2 involvement in stemness (Fig. S3A–F).

In summary, our findings demonstrated that in the SH4 melanoma cell line, overexpression of B4GALNT1 as well as its main products GM2/GD2 promotes AIG and cell migration *in vitro* and enhances tumor incidence by inducing angiogenesis *in vivo*. To our best knowledge, this is the first time that RNA-Seq was performed to elucidate the influence of B4GALNT1. This result indicates that GM2/GD2 or B4GALNT1 is upstream regulator of periostin, and it might cause some change of characters related to tumorigenesis mentioned above in melanoma cell line. In this study, we have not only shown how GM2/GD2 exacerbates tumors' malignant characters by using B4GALNT1 artificial expression system, but also reconfirmed RNA-Seq is useful tool to find novel potential target in cancer.

Materials and Methods

All experiments were performed in accordance with relevant guidelines and regulations.

Cell lines. Human melanoma cell lines (A375, RPMI-7951, SH4 and WM115) were purchased from American Type Culture Collection (Manassas, USA). Human neuroblastoma cell lines (IMR32 and RTBM1) were provided by Dr. Hajime Hosoi (Kyoto Prefectural University of Medicine, Japan). The melanoma cell lines were maintained in Dulbecco's modified Eagle's high-glucose medium (DMEM, Corning, USA) and neuroblastoma cell lines were maintained in Eagle's minimal essential medium (EMEM, Corning) supplemented with 10% FBS, 100 U/ml penicillin and 10 mg/ml streptomycin (Corning). HUVEC was maintained in Endothelial Cell Growth Media (Sigma-Aldrich, USA). All cells were cultured at 37 °C in a humidified atmosphere of 5% CO_2.

Construction of a cDNA expression vector, gene transfection and selection. Human *B4GALNT1* cDNA was cloned from IMR32 with the primers listed in Table S3. The fragment was first inserted into Topo vector using Zero Blunt TOPO PCR Cloning Kit (Invitrogen, USA). After confirmation of sequence, the cDNA cut out by BamHI and NotI was inserted into the cDNA3.1(+) expression vector (Invitrogen). SH4 cells were plated in a 60-mm plastic plate (Corning) and then transfected with the plasmids by using Superfect (Qiagen, Germany). Stable transfectants were isolated in the presence of 600 μg/ml G418 (Roche, Germany).

Flow cytometric analysis. Cells were trypsinized and washed twice with flow cytometry buffer (FCB, PBS supplemented with 1% FBS and 0.02% sodium azide (Sigma-Aldrich)). Cells were incubated with the anti-hGD2 mAbs (MAB2052, Millipore, USA) and anti-hABCB5 mAbs (MA5-17026, Thermo Fischer Scientific, USA (1:100, 100 μl/10^6 cells) for 1 h and then washed in FCB. The cells were subsequently incubated with FITC-labeled anti-mouse goat IgG (sc-2010; 1:1,000, 1 ml/10^6 cells, Santa Cruz Biotechnology, USA) for 40 min, and washed twice with FCB. Cells were incubated in PE-conjugated anti-hCD133/2 mAbs (#130-090-853, Miltenyi Biotec, Germany), PE-conjugated anti-hALCAM/CD166 mAbs (#105902, R&D systems, USA) and FITC-conjugated anti-hCD271/NGFR antibody (#345103, BioLegend, USA), (1:200, 1 ml/10^6 cells) for 15 min and then washed with FCB. With PE-conjugated anti-hNestin mAbs (#196908, R&D systems), cells (1×10^6 cells/200 μl) were fixed with 200 μl of cold 4% paraformaldehyde (Sigma-Aldrich) at room temperature for 30 min, and then washed in FCB twice. After incubation with 500 μl 0.1% Triton X-100 (Sigma-Aldrich) for 10 min at room temperature, cells were washed with FCB twice and stained with the antibody (1:200, 1 ml/10^6 cells) on ice for 30 min in the dark, and subsequently washed with FCB. ALDH activity was determined by ALDEFLUOR Kit (Stemcell Technologies, Canada) according to the manufacturer's instructions. All procedures were performed at 4 °C. The samples were immediately analyzed using FACS Canto II flow cytometer (BD Bioscience, USA). In each sample at least 1×10^4 events were collected. The data was analyzed with FlowJo software (FlowJo, LLC, USA).

High-performance liquid chromatography (HPLC). HPLC was carried out as described previously[68–70]. Briefly, the acidic glycosphingolipids were extracted from each melanoma and neuroblastoma cell

line (1×10^6 cells) and digested with recombinant endoglycoceramidase II from Rhodococcus sp. (Takara Bio, Japan). The released oligosaccharides were labeled with 2-aminopyridine and separated using a HPLC system equipped with a fluorescence detector. Normal-phase HPLC was performed on a TSK gel Amide-80 column (Tosoh, Japan). The molecular size of each PA-oligosaccharide is given in glucose units (Gu) based on the elution times of PA-isomaltooligosaccharides. Reversed-phase HPLC was performed on a TSK gel ODS-80Ts column (Tosoh). The retention time of each PA-oligosaccharide is given in glucose units based on the elution times of PA-isomaltooligosaccharides. Thus, a given compound on these two columns provides a unique set of Gu (amide) and Gu (ODS) values, which correspond to coordinates of the 2-D map. PA-oligosaccharides were analyzed using LC/ESI MS/MS. Standard PA-oligosaccharides, PA-GM1 and PA-GD1a, were purchased from Takara Bio and PA-LST-a and PA-SPG were obtained from our previous study[71].

Real time RT–PCR. Total RNA was extracted from a tumor specimen with RNeasy mini kit (Qiagen) and complementary DNA (cDNA) was synthesized by the use of the SuperScript VILO cDNA Synthesis Kit (Thermo Fisher Scientific) according to the manufacturer's instructions, respectively. The primers used in this experiment are listed in Table S3. Real-time RT-PCR was carried out using LightCycler 480 System (Roche) with SYBR Green (Applied Biosystems, CA) as previously described[72]. Thermal cycling conditions were: initial denaturation for 10 min at 95 °C, and 40 cycles of 15 sec at 95 °C, and 1 min at 60 °C. Data were analyzed with the Light Cycler software.

Assay for cell proliferation. Cells were seeded at 2×10^4 cells/well in 12-well plate. Every 48 h, cells were dissociated by 0.25% trypsin (Corning) and neutralized by the same volume of 10% DMEM. After that 100 µl 0.5% trypan blue (Sigma-Aldrich) and counted by Cellometer Auto T4 (Nexcelom Bioscience, USA) until days 6.

Anchorage-independent soft agar colony formation assay. Cells were cultured in a two-layer soft agar system[73]. It consisted of a 1% agarose (RPI, USA) underlayer and a 0.7% agarose overlayer containing 1×10^4 cells in 60-mm dishes (Corning). Colonies were allowed to form for 2 weeks with fresh media added every 3 days. Plates were stained with crystal violet and colonies more than 0.1 mm in diameter were counted.

Wound-healing assay. Wound-healing assays were carried out as described previously[74,75]. Immediately after scratching (0 h), the plates were photographed and the distance between the edges of the wound area was measured. At 6 h and 24 h after scratching, the plates were photographed and the distance between the edges of the wound region was again measured.

***In vivo* tumorigenesis.** Tumors were induced in 5–6 week old female and male NSG mice (Jackson Laboratory, USA). Each mouse was injected subcutaneously with SH4 cell lines transformed with pcDNA3.1(+) empty vector or the one expressing *B4GALNT1* suspended in 0.1 ml of PBS at a single site (2×10^6 cell; left, 2×10^5 cell; right) to the lower flank. Tumor diameter was monitored every 2–3 days on onset of tumor formation. Mice were sacrificed when the largest tumor size reached 16 mm in diameter along with IACUC approved protocol. At the end point of the experiments, tumors were extracted. At least 4 mice were used in each group (Mock, #4 and #5). The animal experiments were performed in accordance with the institutionally approved animal experimental protocol.

Histopathology and immunohistochemistry. Histological specimens were fixed in 10% formalin and routinely processed for embedding in paraffin. The sections were stained with H&E. Some portions of tumors were embedded in OCT and frozen at −20 °C for immunofluorescence analyses. The tumors were sectioned 30-µm-thick by CM 1800 Cryostat (Leica Biosystems, Germany). The sections were fixed by 50 µl of ice-cold acetone for 5 min. After washing the slides in 1 x PBS, they were incubated in blocking buffer (2% bovine serum albumin (BSA) serum in PBS) for 1 h. The sections were incubated with PE-conjugated anti-mouse CD31 antibody (#102507, BioLegend, 1:500 at 4 °C overnight). After washing the slides in 1 x PBS three times, the slides were incubated by 20 µl VECTASHIELD Antifade Mounting Medium with DAPI (H-1200, Vector Laboratories, USA) and coverslipped. The tissues were observed with automated upright microscope System DM5500 B (Leica Biosystems).

RNA sequencing (whole transcriptome shotgun sequencing, WTSS) and analysis. RNAs derived from SH4 with (#4 and #5) or without (Mock; two samples) *B4GALNT1* over-expression were analyzed by RNA sequencing as described in ref. [76–78]. Quality tested with Bioanalyzer 2100 (Agilent Technologies, USA). Sequencing was accomplished on the MiSeq 500 (Illumina, USA). 50 bp FastQ paired-end reads (n = 23.6 Million per sample) were trimmed using Trimmomatic (v 0.33). Quality control checks on raw sequence data were performed with FastQC. Read mapping was performed via Hisat2 (2.1.0) using the Human UCSC genome (hg38) as reference. Differentially expressed genes were identified using the edgeR (Bioconductor, www.bioconductor.org) feature in CLCGWB (Qiagen) using raw read counts. The generated list was filtered based on a minimum 2 x absolute fold change and false discovery rate (FDR) corrected $p < 0.05$. Pathway analysis was performed in IPA (Qiagen) using fold change and FDR corrected values.

Statistical analysis. Statistical analysis was performed using the unpaired Student's t-test. A P-value of less than 0.05 was considered statistically significant.

Received: 19 September 2019; Accepted: 22 November 2019;
Published online: 27 January 2020

References

1. Linos, E., Swetter, S. M., Cockburn, M. G., Colditz, G. A. & Clarke, C. A. Increasing burden of melanoma in the United States. *Journal of Investigative Dermatology* **129**, 1666–1674 (2009).
2. Erdei, E. & Torres, S. M. A new understanding in the epidemiology of melanoma. *Expert review of anticancer therapy* **10**, 1811–1823 (2010).
3. Rigel, D. S. & Carucci, J. A. Malignant melanoma: prevention, early detection, and treatment in the 21st century. *CA: a cancer journal for clinicians* **50**, 215–236 (2000).
4. Kosary, C. L., Altekruse, S. F., Ruhl, J., Lee, R. & Dickie, L. Clinical and prognostic factors for melanoma of the skin using SEER registries: collaborative stage data collection system, version 1 and version 2. *Cancer* **120**, 3807–3814 (2014).
5. Ernst, D. S. *et al*. Burden of illness for metastatic melanoma in Canada, 2011–2013. *Current Oncology* **23**, e563 (2016).
6. Szczepaniak Sloane, R. A. *et al*. Interaction of molecular alterations with immune response in melanoma. *Cancer* **123**, 2130–2142 (2017).
7. Robert, C. *et al*. Ipilimumab plus dacarbazine for previously untreated metastatic melanoma. *New England Journal of Medicine* **364**, 2517–2526 (2011).
8. Spain, L., Julve, M. & Larkin, J. Combination dabrafenib and trametinib in the management of advanced melanoma with BRAFV600 mutations. *Expert opinion on pharmacotherapy* **17**, 1031–1038 (2016).
9. Wood, K. & Luke, J. J. Optimal use of BRAF targeting therapy in the immunotherapy era. *Current oncology reports* **18**, 67 (2016).
10. Callahan, M. K., Postow, M. A. & Wolchok, J. D. Immunomodulatory therapy for melanoma: ipilimumab and beyond. *Clinics in dermatology* **31**, 191–199 (2013).
11. Ascierto, P. A. *et al*. The role of BRAF V600 mutation in melanoma. *Journal of translational medicine* **10**, 85 (2012).
12. Hodi, F. S. *et al*. Combined nivolumab and ipilimumab versus ipilimumab alone in patients with advanced melanoma: 2-year overall survival outcomes in a multicentre, randomised, controlled, phase 2 trial. *The Lancet Oncology* **17**, 1558–1568 (2016).
13. Kholodenko, I. V., Kalinovsky, D. V., Doronin, I. I., Deyev, S. M. & Kholodenko, R. V. Neuroblastoma origin and therapeutic targets for immunotherapy. *Journal of immunology research* **2018**, 7394268 (2018).
14. Kolter, T. Ganglioside biochemistry. *ISRN biochemistry* **2012**, 506160 (2012).
15. Robert, K. Y., Nakatani, Y. & Yanagisawa, M. The role of glycosphingolipid metabolism in the developing brain. *Journal of lipid research* **50**, S440–S445 (2009).
16. Hoon, D. S. B., Irie, R. F. & Cochran, A. J. Gangliosides from human melanoma immunomodulate response of T cells to interleukin-2. *Cellular immunology* **111**, 410–419 (1988).
17. Todeschini, A. R. & Hakomori, S.-I. Functional role of glycosphingolipids and gangliosides in control of cell adhesion, motility, and growth, through glycosynaptic microdomains. *Biochimica et Biophysica Acta (BBA)-General Subjects* **1780**, 421–433 (2008).
18. Ledeen, R. W. & Wu, G. Ganglioside function in calcium homeostasis and signaling. *Neurochemical research* **27**, 637–647 (2002).
19. Hakomori, S.-I. Traveling for the glycosphingolipid path. *Glycoconjugate journal* **17**, 627–647 (2000).
20. Hakomori, S.-I. Tumor malignancy defined by aberrant glycosylation and sphingo (glyco) lipid metabolism. *Cancer research* **56**, 5309–5318 (1996).
21. Cheung, I. Y., Lo Piccolo, M. S., Kushner, B. H. & Cheung, N.-K. V. Early molecular response of marrow disease to biologic therapy is highly prognostic in neuroblastoma. *Journal of clinical oncology* **21**, 3853–3858 (2003).
22. Tringali, C. *et al*. Molecular subtyping of metastatic melanoma based on cell ganglioside metabolism profiles. *BMC cancer* **14**, 560 (2014).
23. Modak, S., Gerald, W. & Cheung, N. K. V. Disialoganglioside GD2 and a novel tumor antigen: potential targets for immunotherapy of desmoplastic small round cell tumor. *Medical and pediatric oncology* **39**, 547–551 (2002).
24. Tsuchida, T., Saxton, R. E., Morton, D. L. & Irie, R. F. Gangliosides of human melanoma. *JNCI: Journal of the National Cancer Institute* **78**, 45–54 (1987).
25. Chang, H. R., Cordon-Cardo, C., Houghton, A. N., Cheung, N. K. V. & Brennan, M. F. Expression of disialogangliosides GD2 and GD3 on human soft tissue sarcomas. *Cancer* **70**, 633–638 (1992).
26. Heiner, J. P. *et al*. Localization of GD2-specific monoclonal antibody 3F8 in human osteosarcoma. *Cancer Research* **47**, 5377–5381 (1987).
27. Wu, Z.-L., Schwartz, E., Seeger, R. & Ladisch, S. Expression of GD2 ganglioside by untreated primary human neuroblastomas. *Cancer research* **46**, 440–443 (1986).
28. Sasaki, K. *et al*. Expression cloning of a GM3-specific alpha-2, 8-sialyltransferase (GD3 synthase). *Journal of Biological Chemistry* **269**, 15950–15956 (1994).
29. Klein, W. M. *et al*. Increased expression of stem cell markers in malignant melanoma. *Modern pathology* **20**, 102–107 (2007).
30. Sabet, M. N., Rakhshan, A., Erfani, E. & Madjd, Z. Co-expression of putative cancer stem cell markers, CD133 and Nestin, in skin tumors. *Asian Pacific Journal of Cancer Prevention* **15**, 8161–8169 (2014).
31. Roudi, R. *et al*. Comparative gene-expression profiling of CD133+ and CD133-D10 melanoma cells. *Future*. *Oncology* **11**, 2383–2393 (2015).
32. Redmer, T. *et al*. The role of the cancer stem cell marker CD271 in DNA damage response and drug resistance of melanoma cells. *Oncogenesis* **6**, e291 (2017).
33. Wilson, B. J. *et al*. ABCB5 maintains melanoma-initiating cells through a pro-inflammatory cytokine signaling circuit. *Cancer research* **74**, 4196–4207 (2014).
34. Luo, Y. *et al*. ALDH1A isozymes are markers of human melanoma stem cells and potential therapeutic targets. *Stem cells* **30**, 2100–2113 (2012).
35. Veeriah, S. *et al*. The tyrosine phosphatase PTPRD is a tumor suppressor that is frequently inactivated and mutated in glioblastoma and other human cancers. *Proceedings of the National Academy of Sciences* **106**, 9435–9440 (2009).
36. Liu, A. Y., Zheng, H. & Ouyang, G. Periostin, a multifunctional matricellular protein in inflammatory and tumor microenvironments. *Matrix biology* **37**, 150–156 (2014).
37. Zheng, Q.-m *et al*. Periostin facilitates the epithelial-mesenchymal transition of endometrial epithelial cells through ILK-Akt signaling pathway. *BioMed research international* **2016**, 9842619 (2016).
38. Ruan, K., Bao, S. & Ouyang, G. The multifaceted role of periostin in tumorigenesis. *Cellular and molecular life sciences* **66**, 2219–2230 (2009).
39. Mahoney, J. A., Ntolosi, B., DaSilva, R. P., Gordon, S. & McKnight, A. J. Cloning and characterization of CPVL, a novel serine carboxypeptidase, from human macrophages. *Genomics* **72**, 243–251 (2001).
40. Zhao, G. *et al*. Overexpression and Implications of Melanoma-associated Antigen A12 in Pathogenesis of Human Cutaneous Squamous Cell Carcinoma. *Anticancer research* **39**, 1849–1857 (2019).
41. Lin, C. *et al*. Cancer/testis antigen CSAGE is concurrently expressed with MAGE in chondrosarcoma. *Gene* **285**, 269–278 (2002).
42. Mahata, B., Banerjee, A., Kundu, M., Bandyopadhyay, U. & Biswas, K. TALEN mediated targeted editing of GM2/GD2-synthase gene modulates anchorage independent growth by reducing anoikis resistance in mouse tumor cells. *Scientific reports* **5**, 9048 (2015).
43. Mori, S. *et al*. Anchorage-independent cell growth signature identifies tumors with metastatic potential. *Oncogene* **28**, 2796–2805 (2009).
44. Colburn, N. H. *et al*. Correlation of anchorage-independent growth with tumorigenicity of chemically transformed mouse epidermal cells. *Cancer research* **38**, 624–634 (1978).

45. Lai, J.-P., Sandhu, D. S., Shire, A. M. & Roberts, L. R. The tumor suppressor function of human sulfatase 1 (SULF1) in carcinogenesis. *Journal of gastrointestinal cancer* **39**, 149–158 (2008).
46. Kalus, I. *et al*. Sulf1 and Sulf2 differentially modulate heparan sulfate proteoglycan sulfation during postnatal cerebellum development: evidence for neuroprotective and neurite outgrowth promoting functions. *PLoS One* **10**, e0139853 (2015).
47. Conway, S. J. *et al*. The role of periostin in tissue remodeling across health and disease. *Cellular and Molecular Life Sciences* **71**, 1279–1288 (2014).
48. Kudo, Y. *et al*. Periostin promotes invasion and anchorage-independent growth in the metastatic process of head and neck cancer. *Cancer research* **66**, 6928–6935 (2006).
49. Kotobuki, Y. *et al*. Periostin accelerates human malignant melanoma progression by modifying the melanoma microenvironment. *Pigment cell & melanoma research* **27**, 630–639 (2014).
50. Fukuda, K. *et al*. Periostin is a key niche component for wound metastasis of melanoma. *PloS one* **10**, e0129704 (2015).
51. Bao, S. *et al*. Periostin potently promotes metastatic growth of colon cancer by augmenting cell survival via the Akt/PKB pathway. *Cancer cell* **5**, 329–339 (2004).
52. Yoshida, S. *et al*. Ganglioside GD2 in small cell lung cancer cell lines: enhancement of cell proliferation and mediation of apoptosis. *Cancer research* **61**, 4244–4252 (2001).
53. Hamamura, K. *et al*. Ganglioside GD3 promotes cell growth and invasion through p130Cas and paxillin in malignant melanoma cells. *Proceedings of the National Academy of Sciences* **102**, 11041–11046 (2005).
54. Liu, Y. *et al*. Ganglioside synthase knockout in oncogene-transformed fibroblasts depletes gangliosides and impairs tumor growth. *Oncogene* **29**, 3297–3306 (2010).
55. Shibuya, H. *et al*. Enhancement of malignant properties of human osteosarcoma cells with disialyl gangliosides GD 2/GD 3. *Cancer science* **103**, 1656–1664 (2012).
56. Tang, Y. *et al*. Periostin promotes migration and osteogenic differentiation of human periodontal ligament mesenchymal stem cells via the Jun amino-terminal kinases (JNK) pathway under inflammatory conditions. *Cell proliferation* **50**, e12369 (2017).
57. Gillan, L. *et al*. Periostin secreted by epithelial ovarian carcinoma is a ligand for αVβ3 and αVβ5 integrins and promotes cell motility. *Cancer research* **62**, 5358–5364 (2002).
58. Li, G. *et al*. Periostin mediates vascular smooth muscle cell migration through the integrins αvβ3 and αvβ5 and focal adhesion kinase (FAK) pathway. *Atherosclerosis* **208**, 358–365 (2010).
59. Kuo, C. T. *et al*. Assessment of messenger RNA of beta 1–>4-N-acetylgalactosaminyl-transferase as a molecular marker for metastatic melanoma. *Clinical Cancer Research* **4**, 411–418 (1998).
60. Liu, Y., Wondimu, A., Yan, S., Bobb, D. & Ladisch, S. Tumor gangliosides accelerate murine tumor angiogenesis. *Angiogenesis* **17**, 563–571 (2014).
61. Lang, Z., Guerrera, M., Li, R. & Ladisch, S. Ganglioside GD1a enhances VEGF-induced endothelial cell proliferation and migration. *Biochemical and biophysical research communications* **282**, 1031–1037 (2001).
62. Chung, T.-W. *et al*. Ganglioside GM3 inhibits VEGF/VEGFR-2-mediated angiogenesis: direct interaction of GM3 with VEGFR-2. *Glycobiology* **19**, 229–239 (2008).
63. Liu, Y. *et al*. Periostin promotes tumor angiogenesis in pancreatic cancer via Erk/VEGF signaling. *Oncotarget* **7**, 40148–40159 (2016).
64. Siriwardena, B. *et al*. Periostin is frequently overexpressed and enhances invasion and angiogenesis in oral cancer. *British journal of cancer* **95**, 1396–1403 (2006).
65. Liu, Y., McCarthy, J. & Ladisch, S. Membrane ganglioside enrichment lowers the threshold for vascular endothelial cell angiogenic signaling. *Cancer research* **66**, 10408–10414 (2006).
66. Liang, Y.-J. *et al*. Differential expression profiles of glycosphingolipids in human breast cancer stem cells vs. cancer non-stem cells. *Proceedings of the National Academy of Sciences* **110**, 4968–4973 (2013).
67. Liang, Y.-J. *et al*. Interaction of glycosphingolipids GD3 and GD2 with growth factor receptors maintains breast cancer stem cell phenotype. *Oncotarget* **8**, 47454–47473 (2017).
68. Nomura, M., Shimbo, T., Miyamoto, Y., Fukuzawa, M. & Kaneda, Y. 13-Cis retinoic acid can enhance the antitumor activity of non-replicating S endai virus particle against neuroblastoma. *Cancer science* **104**, 238–244 (2013).
69. Kawaguchi, Y., Miyamoto, Y., Inoue, T. & Kaneda, Y. Efficient eradication of hormone-resistant human prostate cancers by inactivated Sendai virus particle. *International journal of cancer* **124**, 2478–2487 (2009).
70. Hatano, K., Miyamoto, Y., Nonomura, N. & Kaneda, Y. Expression of gangliosides, GD1a, and sialyl paragloboside is regulated by NF-κB-dependent transcriptional control of α2, 3-sialyltransferase I, II, and VI in human castration-resistant prostate cancer cells. *International journal of cancer* **129**, 1838–1847 (2011).
71. Korekane, H. *et al*. Novel fucogangliosides found in human colon adenocarcinoma tissues by means of glycomic analysis. *Analytical biochemistry* **364**, 37–50 (2007).
72. Yoshida, H. *et al*. Post-transcriptional modulation of C/EBPα prompts monocytic differentiation and apoptosis in acute myelomonocytic leukaemia cells. *Leukemia research* **36**, 735–741 (2012).
73. Hamburger, A. W. *et al*. Direct cloning of human ovarian carcinoma cells in agar. *Cancer research* **38**, 3438–3444 (1978).
74. Yoshida, H. *et al*. PAX3-NCOA2 fusion gene has a dual role in promoting the proliferation and inhibiting the myogenic differentiation of rhabdomyosarcoma cells. *Oncogene* **33**, 5601–5608 (2014).
75. Kikuchi, K. *et al*. Effects of PAX3-FKHR on malignant phenotypes in alveolar rhabdomyosarcoma. *Biochemical and biophysical research communications* **365**, 568–574 (2008).
76. Rathe, S. K. *et al*. Using RNA-seq and targeted nucleases to identify mechanisms of drug resistance in acute myeloid leukemia. *Scientific reports* **4**, 6048 (2014).
77. Dauer, P. *et al*. Inactivation of cancer-associated-fibroblasts disrupts oncogenic signaling in pancreatic cancer cells and promotes its regression. *Cancer research* **78**, 1321–1333 (2018).
78. Clark, C. R. *et al*. Transposon mutagenesis screen in mice identifies TM9SF2 as a novel colorectal cancer oncogene. *Scientific reports* **8**, 15327 (2018).

Acknowledgements

This research was partly supported by grants from NIH/NCI (R01CA168448 and R01CA196215 to MY), and the Research Support from Department of Surgery, University of Minnesota. .

Author contributions

Conception and design: H. Yoshida and M. Yamamoto. Development of methodology: H. Yoshida, L. Koodie, Y. Miyamoto, and M. Yamamoto. Acquisition of data (provide): H. Yoshida (All), L. Koodie (Immunostaining), K. Jacobsen (Animal experiments), and K. Hanzawa (Glycobiology). Analysis and interpretation of data: H. Yoshida and M. Yamamoto. Writing review, and/or revision of the manuscript: H. Yoshida and M. Yamamoto. Administrative, technical, or material support: L. Koodie and K. Jacobsen. Study supervision: M. Yamamoto.

Competing interests
The authors declare no competing interests.

Additional information
Supplementary information is available for this paper at https://doi.org/10.1038/s41598-019-57130-2.

Correspondence and requests for materials should be addressed to M.Y.

Reprints and permissions information is available at www.nature.com/reprints.

Publisher's note Springer Nature remains neutral with regard to jurisdictional claims in published maps and institutional affiliations.

Open Access This article is licensed under a Creative Commons Attribution 4.0 International License, which permits use, sharing, adaptation, distribution and reproduction in any medium or format, as long as you give appropriate credit to the original author(s) and the source, provide a link to the Creative Commons license, and indicate if changes were made. The images or other third party material in this article are included in the article's Creative Commons license, unless indicated otherwise in a credit line to the material. If material is not included in the article's Creative Commons license and your intended use is not permitted by statutory regulation or exceeds the permitted use, you will need to obtain permission directly from the copyright holder. To view a copy of this license, visit http://creativecommons.org/licenses/by/4.0/.

© The Author(s) 2020